High-Q Exterior Whispering-Gallery Modes in a Double-Layer Crystalline Microdisk Resonator

Yuanlin Zheng,[1,2,*] Zhiwei Fang,[3,4,5,*] Shijie Liu,[1,2] Ya Cheng,[3,4,5,6,‡] and Xianfeng Chen[1,2,†]

[1]*State Key Laboratory of Advanced Optical Communication Systems and Networks, School of Physics and Astronomy, Shanghai Jiao Tong University, Shanghai 200240, China*

[2]*Key Laboratory for Laser Plasma (Ministry of Education), Collaborative Innovation Center of IFSA, Shanghai Jiao Tong University, Shanghai 200240, China*

[3]*State Key Laboratory of Precision Spectroscopy, East China Normal University, Shanghai 200062, China*

[4]*XXL-The Extreme Optoelectromechanics Laboratory, School of Physics and Materials Science, East China Normal University, Shanghai 200241, China*

[5]*State Key Laboratory of High Field Laser Physics, Shanghai Institute of Optics and Fine Mechanics, Chinese Academy of Sciences, Shanghai 201800, China*

[6]*Collaborative Innovation Center of Extreme Optics, Shanxi University, Taiyuan, Shanxi 030006, China*

(Received 11 April 2019; published 27 June 2019)

Exterior whispering-gallery modes (WGMs), whose mode energy is mainly confined outside the microcavity, can achieve large mode overlapping with the ambient environment, as well as a strong electric field and gradient force at the surface. Here, we demonstrate highly localized WGMs in the nanoair gap of a double-layer crystalline microdisk. The geometry is based on a horizontal slot-waveguide structure of two vertically stacked crystalline microdisks made of lithium niobate thin films. The slot WGM possesses a high quality factor in excess of 10^5 without metallic loss. The absorption and scattering loss is reduced by use of the crystalline nanofilm at sub-nm rms surface roughness. The demonstrated configuration can be highly favored in various applications including optical sensing, nonlinear optics, and optomechanics.

DOI: 10.1103/PhysRevLett.122.253902

Whispering-gallery-mode (WGM) microresonators underpin a breath of important applications in optical sensing, nonlinear optics, optomechanics, and quantum optics [1–4]. High-Q (quality) microcavities with various geometries have been demonstrated, such as microspheres, microtoroids, microbottles, and microdisks. Conventionally, WGMs are dominantly confined inside high-refractive-index dielectric microcavities via total internal reflection (TIR), with a small portion of mode energy extended into the ambient environment (i.e., evanescent field) for both light coupling and optical sensing.

In contrast, exterior WGMs have been long sought after for optical sensing applications due to their large mode overlap with the surroundings and thus more sensitive to perturbation. Typically, they can be excited by utilizing plasmonic resonant cavities [5,6] and slot-waveguide structures [7–9]. The plasmonic microcavity can confine the electromagnetic field down to a much smaller mode volume (V) by taking advantage of surface plasmon resonance (SPR). However, the large intrinsic metallic loss greatly degrades their Q factors, with the highest theoretical Q factors to only about 10^3 [5,6]. Hybrid schemes have therefore been proposed, e.g., by attaching metallic nanoparticles (NPs) to dielectric microcavities [10]. But the long-standing problem of metallic loss in SPR is, in principle, unavoidable. Another way to achieve exterior WGMs is based on slot-waveguide structures, in which the excited modes are confined in between a nanogap (slot) of two closely placed dielectric media, e.g., planar slot-waveguide ring resonators [11]. Light confinement and enhancement is caused by large discontinuity of the electric field at high-index-contrast interfaces [12], rather than TIR or SPR. However, the subwavelength vertical slot structure requires high-precision fabrication techniques, for instance, electron beam lithography (EBL) and the dry etching method. Slot-waveguide modes are known to be vulnerable to roughness induced extrinsic scattering, which imposes their main loss. The fabrication of a vertical nanoslot with high aspect ratios and ultrasmooth sidewalls is still a challenge and at high cost. To date, the highest quality factor reported in silicon vertical slot waveguide microring resonators with careful design and fabrication is of the order of 10^4 at 1550 nm [9]. To overcome these drawbacks, horizontal slot-waveguide schemes have been utilized for better gap control [13]. But, the mature nanofabrication technique for both geometries is still limited to CMOS compatible materials, most of which lack second-order nonlinearity.

Here, we demonstrate that a double-layer crystalline microdisk supports exterior slot WGMs with high-Q factors. The geometry consists of two vertically stacked lithium niobate thin film (LNTF) microdisks separated by a nanoscale gap, and forms a horizontal slot-waveguide

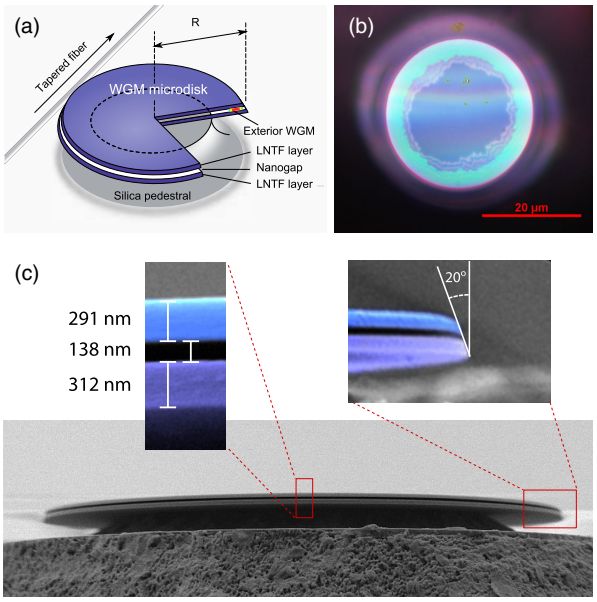

FIG. 1. (a) Schematic of the double-layer LNOI microdisk evanescently coupled by a tapered fiber. (b) Top-view optical microscopy image of the microdisk. The two inner irregularly shaped circles indicate inward etching of the silica buffer layers. (c) SEM image of the microdisk, with enlarged false-colored images clearly showing the well-separated upper and lower LNTF layers.

microdisk resonator. The microcavity features high-Q slot WGMs, in excess of 10^5, at the telecommunication C band. Our configuration on the double-layered lithium niobate on insulator (LNOI) platform would also be beneficial for novel effects with the material's exceptional properties, e.g., optical nonlinearity, electro-optics, and piezoelectricity.

The geometry of the double-layer LNOI microdisk is sketched in Fig. 1(a). The microdisk has a radius (R) of 15 μm, and is evanescently coupled using a tapered fiber (diameter $\sim$2 μm) in contact with its outer rim. The stacked microdisk sample is fabricated from a customized two layer x-cut LNOI chip, with one layer of LNOI on top of the other (*NANOLN* Co.). The fabrication method is femtosecond laser direct writing followed by a focused ion beam (FIB) milling procedure, the same as previous reports [14–16]. After the fabrication of the microdisk, the silica buffer layers are selectively etched by HF acid, to form a pedestal for the microcavity and also a nanoair gap between the two vertically stacked LNOI microdisks. The thickness of the five layers of the chip from top down is 291 nm (LN), 138 nm (silica), 312 nm (LN), 2 μm (silica), and 0.5 mm (LN), respectively. A top-view optical microscopy image of the fabricated double-layer LNOI microdisk is shown in Fig. 1(b). The two inner irregularly shaped circles belong to silica buffering layers partially removed to form a pedestal for the microdisk and the nanogap in between. As can be seen, the depth of the slot is more than 5 μm, larger than the width of WGMs. A side-view scanning electron microscopy (SEM) image is presented in Fig. 1(c), which reveals details of the double-layer LNOI microdisk, and by which the exact thickness of each layer is determined. From the SEM image and enlarged false-colored ones, one can find that a uniform nanogap is formed in between the two stacked LNOI microdisks with a wedge angle of approximately 20°.

Since WGMs are confined to the rim of microcavities, they are sensitive to scattering by surface roughness that might be introduced during FIB milling. Because the microdisk's edge is suspended in air and possesses a large wedge angle, it is difficult to directly image the topography at the rim of the LNOI microdisk by atomic force microscopy (AFM). Instead, we fabricated in a 700-nm thick LNOI film a square pit using FIB milling. The fabrication methods and parameters are kept the same for the two fabrication processes. Figure 2(a) shows the microscopy image of the square pit with a dimension of 10×10 μm^2. We measured both the surface roughness of the LNOI film and the FIB etched pit by randomly selecting a spot at one pit edge. The measured result of the surface and sidewall by AFM is reconstructed in Fig. 2(b). The measured surface, as marked by the red dashed square in Fig. 2(a), occupies an area of approximately 2×2 μm^2 by which the roughness calculation is performed. The etched depth of the pit is 390 nm. The surface roughness of the LNTF by chemomechanical polishing is 0.25 nm rms, and that by FIB milling is 0.3 nm rms. The roughness at the slope is 0.5 nm rms, still in the sub-nm level. This proves super smoothness of the LNOI microdisk to achieve low scattering induced loss.

To theoretically investigate different kinds of supported WGMs, a finite-element analysis was performed for the double-layer LNOI microdisk to find their mode profiles. Figure 3 shows the energy distribution of found typical interior and exterior modes. The wedge angle and each dimension of the microdisk sample are based on the cross-sectional SEM image of the microdisk [Fig. 1(c)]. The crystalline optical axis is along the z axis. In Fig. 3(a), we display a typical interior WGM inside the cavity, which dominantly exhibits quasi-TE modes due to a thin geometry. The characteristics of these kinds of modes

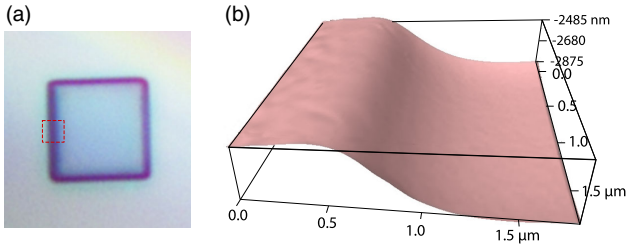

FIG. 2. (a) Optical microscopic image of the top surface of a LNOI chip with a square pit fabricated by FIB milling. The pit area is 10×10 μm^2. (b) AFM reconstruction of the surface as marked by the red square in (a), showing ultrasmooth surface (sub-nm rms roughness).

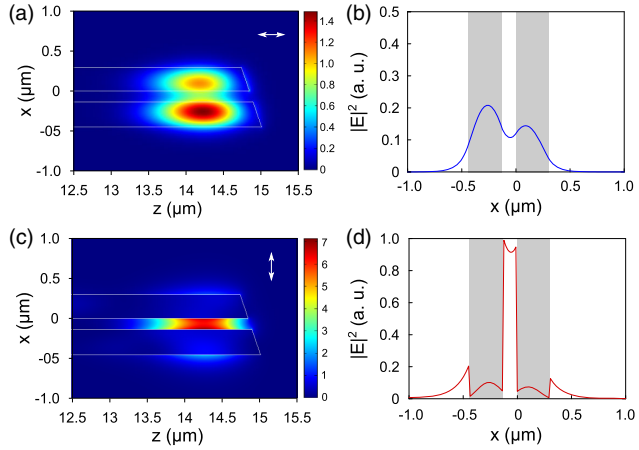

FIG. 3. Transverse intensity profiles ($|E|^2$) of (a) interior WGMs and (c) exterior slot WGMs. White arrows indicate the polarization of the electric field. (b) and (d) The intensity distribution of the respective mode along the z direction. Gray regions correspond to the LNTF layers.

(both symmetric and antisymmetric) are that they exhibit strong optical gradient forces and thus strongly back act with the microcavity, which has been exploited for optomechanics [17–19]. The shown mode has a radial and azimuthal order of (1, 100) at 193.0 THz, and an effective refractive index of 1.65. The effective mode area is $A_{\mathrm{eff}} = (\iint \epsilon(r)|E|^2 dxdy)^2 / \iint \epsilon^2(r)|E|^4 dxdy = 0.86\ \mu\mathrm{m}^2$. From the simulation result, we found 92.9% of its mode energy is confined in the microdisk, 7.1% in the nanogap and the surrounding air. This is calculated by $\iint_S \epsilon(r)|E|^2 dxdy / \iint_\infty \epsilon(r)|E|^2 dxdy$, where S is the region of interest. The percentages vary slightly for different azimuthal mode orders, but still the most energy is stored in the microcavity. This can also be seen by the plot in Fig. 3(b), which shows the intensity profile along the vertical direction (x axis). Estimated from adjacent WGMs, the free-spectral range (FSR) is found to be approximately 12.5 nm. It should be noted that various higher order interior WGMs also exist [16], but are not presented in these simulation results. Yet, for single layer LNOI microdisks of the same thickness (~740 nm) and radius, the evanescent field of the WGM (at the same resonant wavelength) stores only about 1.3% of the total mode energy.

More interestingly, other than the existing interior WGMs, the double-layer LNOI microdisk also supports exterior or slot WGMs. The cross section of the double-layer LNOI microdisk resembles a horizontal slot waveguide, where the electric field normal to the interfaces is enhanced in the slot, i.e., the air nanogap dividing the upper and lower LNTF layers. Figure 3(c) shows a typical quasi-TM slot-waveguide WGM with an order number of (1, 81) at 193.56 THz, whose effective refractive index is 1.37. The effective mode area is calculated to be 1.2 $\mu\mathrm{m}^2$, because more field stretches to the exterior space. As can be seen, a slot depth of only 2.5 μm is sufficient to eliminate the effect of the pedestal on the slot waveguide WGMs. According to the simulation, a much larger portion of the mode energy is confined in the nanoair gap between the two stacked microdisks, about 43.9%. While inside the microdisk, there is 56.1% of the total mode energy. These numbers also vary slightly for different mode orders. A narrower gap would increase the field confined in the slot region, and further reduce the effective mode area. Still, the percentage is much higher than that of interior WGMs, which has only several percentages of mode energy outside the microdisk. The energy distribution along the vertical direction (x axis) is given in Fig. 3(d). The FSR is approximately 13.3 nm. It is worth noticing that during the simulation higher radial order slot-waveguide WGMs can also be found. After comparison, one can see that the slot WGM has superior ability to distribute mode energy outside the microcavity. This is useful for sensitive optical biosensing [20] and sensing of gas [8]. Furthermore, the field gradient is increased due to the sharp disruption of electric field at the interfaces. We envisage that cavity optomechanics would benefit from this enhancement [21].

To investigate the WGMs experimentally, a narrow linewidth external cavity tunable laser was used to scan the pump over a wavelength range of 1530–1570 nm. The laser polarization is controlled by a fiber polarization controller. The sample is placed on a three-dimensional nanostage to finely control its position with respect to the tapered fiber for optical coupling optimization. To avoid the thermal effect, the cavity is pumped using low input power (<100 μW). The taper fiber was in contact with the LNOI microdisk at its outer rim. The experimental measured transmission spectrum is shown in Fig. 4(a). Because of its small dimensions, the mode density is relatively sparse and each mode can be faithfully identified according to the simulation results. In the experiment, the TE/TM mode families can be distinguished by switching the polarization of the input light. This further reduces ambiguity in identification of the WGMs. Each calculated mode is marked in the figure, with fundamental WGMs indicated by blue lines, higher-order WGMs by green and yellow lines, and slot WGMs by red arrows. This is one good match of theoretical perdition and the corresponding experimental result, with some inevitable discrepancy due to sensitive parameters like refractive index and structural dimensions. Still, the measured spectrum matches well with theoretical prediction, indicating that the anticipated slot WGMs have indeed been excited. Overall, the Q factor for interior WGMs is 1.2×10^5, determined with Lorentz curve fitting, as indicated by Fig. 4(b). It corresponds to a fundamental WGM mode [Fig. 3(a)] at an azimuthal order of $m = 99$ at 1567.4 nm. Theoretical calculation of the Q factors based on the absorption coefficient of LN gives an average Q factors

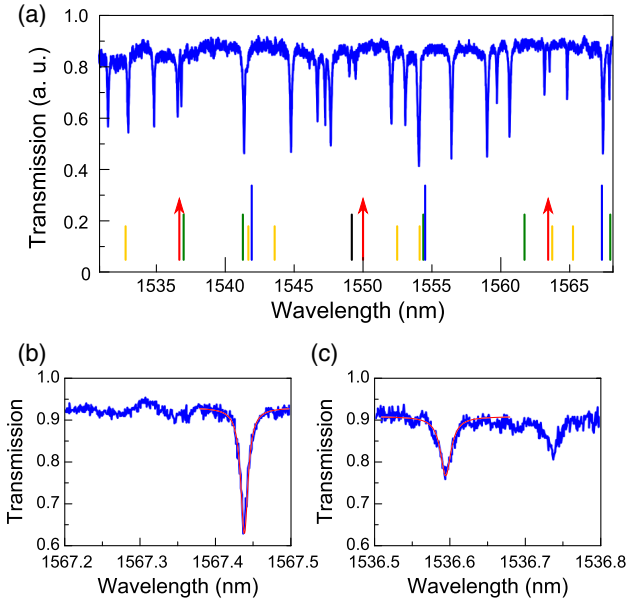

FIG. 4. (a) Experimentally measured transmission spectrum for the double-layer LNOI microdisk. The arrows mark the theoretically predicted slot-waveguide WGMs. (b) Resonance of interior WGM. (c) Resonance of slot-waveguide WGM.

of 10^7, as FIB inevitably introduces lattice imperfection to the material adding further absorption. Thus, there is still improvement that can be achieved in the future. Actually, high Q factors have been reported in LNOI microring and microdisk resonators of the order of 10^7 using the reactive ion etching procedure [22,23].

After analysis, we can determine from the transmission spectrum that exterior slot WGMs were also excited, as marked by arrows in Fig. 4(a). The zoom-in plot of the resonance dip shows a high-Q factor of 1.0×10^5, as indicated by Fig. 4(c). It corresponds to a fundamental slot-waveguide mode [Fig. 3(c)] at an azimuthal order of $m = 82$ at 1536.6 nm. This is 2 orders of magnitude higher than plasmonic WGMs [5,6], also multiple times higher than silicon vertical slot-waveguide ring resonators [9], Si/SiO_2 horizontal slot-waveguide configurations [24], and horizontal air-slot SiNx microdisks of the same geometry [25]. In our case, both interior and slot WGMs show the same order of magnitude in loaded Q factors. This can be straightforward to see, as both types of modes are scattered by the same area of surfaces. It can also be an indicator that the upper and lower boundary of the slot is smooth.

Different from previous reports of slot waveguides, our configuration of double-layer LNOI microdisk possesses several-fold advantages. (i) In horizontal slot waveguides, the gap thickness can be finely defined by thin-film deposition or thermal oxidation with better gap control [13]. This makes horizontal slot waveguides less sensitive to optical scattering losses than vertical configurations. The geometry can also circumvent the difficulty in narrow vertical slot structure fabrication, and more materials can be within choice. (ii) Crystalline structures can have smoother surface and lower absorption coefficients than conventional substrates like silicon, silica, or silicon nitride after the etching process. To date, the record highest Q factors are still achieved using crystalline microcavities [26]. Their surface roughness can reach a sub-nm level via chemo-mechanical polishing. Whereas, dry etching and ion milling inevitably induce imperfection to the structure, e.g., in vertical slot waveguides. But in our geometries, the FIB milled surfaces have limited contact with the slot-waveguide WGMs, and have much smaller impact on their Q factors. (iii) Crystalline materials lacking of inversion symmetry have a strong second-order nonlinearity, which would be further exploited for other photonic applications. Nonlinear optics enhanced by slot-waveguide modes can be investigated. Other materials like silicon, silica, and Si_3N_4 are isotropic, and thus exclude intrinsic second-order nonlinearity (symmetry-breaking induced nonlinearity at surfaces is weak [27]). (iv) Beyond their promising application in optical sensing, cavity optomechanics can also benefit from our scheme. For instance, double-layer microdisks, whose WGMs exhibit strong optical gradient force, have already been exploited for optomechanics [17–19]. Crystalline materials possess a higher Young's module than those porous materials like silica, and would sustain much higher quality mechanical modes, which is an advantage if optomechanics is to be studied. Besides, LNOI microcavities have already been demonstrated to exhibit large frequency-quality product even at room temperature and in atmosphere [28,29], which opens new avenues for studying optomechanics in ambient environments at room temperature.

Although promising, there is much room for further investigation and improvement on the present demonstration. One direction for improvement is to further boost their Q factors to compete conventional ultrahigh-Q microcavities. For instance, Q factors of silica microspheres can routinely reach over the order of 10^7. Yet, the newly developed double-layer crystalline microcavity would still open the door for a wealth of applications in optical sensing and cavity optomechanics. This also holds potential for on-chip nonlinear optics in LNOI photonics by using stacked microcavities. This research will definitely attract intensive interest in the near future.

In conclusion, we have demonstrated horizontal slot WGMs in a double-layer LNOI microdisk, which exhibit a high-Q factor of 10^5. The crystalline double-layer configuration combines the advantages of strong confinement of slot modes, high quality of WGMs, and versatile properties of lithium niobate. Thus, the proposed scheme holds great potential in many applications like optical sensing, nonlinear optics, and optomechanics.

We wish to acknowledge the support of the National Natural Science Foundation of China (NSFC) (11604206,

11734011, 61590934); the National Key R&D Program of China (2018YFA0306301, 2017YFA0303701); and the Foundation for Development of Science and Technology of Shanghai (17JC1400400).

*These authors contributed equally to this work.
†xfchen@sjtu.edu.cn
‡ya.cheng@siom.ac.cn

[1] M. R. Foreman, J. D. Swaim, and F. Vollmer, Whispering gallery mode sensors, Adv. Opt. Photonics **7**, 168 (2015).
[2] G. Lin, A. Coillet, and Y. K. Chembo, Nonlinear photonics with high-Q whispering-gallery-mode resonators, Adv. Opt. Photonics **9**, 828 (2017).
[3] M. Aspelmeyer, T. J. Kippenberg, and F. Marquardt, Cavity optomechanics, Rev. Mod. Phys. **86**, 1391 (2014).
[4] D. V. Strekalov, C. Marquardt, A. B. Matsko, H. G. L. Schwefel, and G. Leuchs, Nonlinear and quantum optics with whispering gallery resonators, J. Opt. **18**, 123002 (2016).
[5] B. Min, E. Ostby, V. Sorger, E. Ulin-Avila, L. Yang, X. Zhang, and K. Vahala, High-Q surface-plasmon-polariton whispering-gallery microcavity, Nature (London) **457**, 455 (2009).
[6] Y. F. Xiao, C. L. Zou, B. B. Li, Y. Li, C. H. Dong, Z. F. Han, and Q. Gong, High-q Exterior Whispering-Gallery Modes in a Metal-Coated Microresonator, Phys. Rev. Lett. **105**, 153902 (2010).
[7] T. Baehr-Jones, M. Hochberg, C. Walker, and A. Scherer, High-Q optical resonators in silicon-on-insulator-based slot waveguides, Appl. Phys. Lett. **86**, 081101 (2005).
[8] J. T. Robinson, L. Chen, and M. Lipson, On-chip gas detection in silicon optical microcavities, Opt. Express **16**, 4296 (2008).
[9] W. Zhang, S. Serna, X. L. Roux, C. Alonso-Ramos, L. Vivien, and E. Cassan, Analysis of silicon-on-insulator slot waveguide ring resonators targeting high-Q-factors, Opt. Lett. **40**, 5566 (2015).
[10] M. D. Baaske and F. Vollmer, Optical observation of single atomic ions interacting with plasmonic nanorods in aqueous solution, Nat. Photonics **10**, 733 (2016).
[11] Q. Xu, V. R. Almeida, R. R. Panepucci, and M. Lipson, Experimental demonstration of guiding and confining light in nanometer-size low-refractive-index material, Opt. Lett. **29**, 1626 (2004).
[12] V. R. Almeida, Q. Xu, C. A. Barrios, and M. Lipson, Guiding and confining light in void nanostructure, Opt. Lett. **29**, 1209 (2004).
[13] R. Sun, P. Dong, N. ning Feng, C. yin Hong, J. Michel, M. Lipson, and L. Kimerling, Horizontal single and multiple slot waveguides: optical transmission at $\lambda = 1550$ nm, Opt. Express **15**, 17967 (2007).
[14] J. Lin, Y. Xu, Z. Fang, M. Wang, J. Song, N. Wang, L. Qiao, W. Fang, and Y. Cheng, Fabrication of high-Q lithium niobate microresonators using femtosecond laser micromachining, Sci. Rep. **5**, 8072 (2015).
[15] Z. Fang, Y. Xu, M. Wang, L. Qiao, J. Lin, W. Fang, and Y. Cheng, Monolithic integration of a lithium niobate microresonator with a free-standing waveguide using femtosecond laser assisted ion beam writing, Sci. Rep. **7**, 45610 (2017).
[16] Z. Fang, N. Yao, M. Wang, J. Lin, J. Zhang, R. Wu, L. Qiao, W. Fang, T. Lu, and Y. Cheng, Fabrication of high quality factor lithium niobate double-disk using a femtosecond laser, Int. J. Optomechatron. **11**, 47 (2017).
[17] G. S. Wiederhecker, L. Chen, A. Gondarenko, and M. Lipson, Controlling photonic structures using optical forces, Nature (London) **462**, 633 (2009).
[18] Q. Lin, J. Rosenberg, X. Jiang, K. J. Vahala, and O. Painter, Mechanical Oscillation and Cooling Actuated by the Optical Gradient Force, Phys. Rev. Lett. **103**, 103601 (2009).
[19] J. Rosenberg, Q. Lin, and O. Painter, Static and dynamic wavelength routing via the gradient optical force, Nat. Photonics **3**, 478 (2009).
[20] S. Lee, S. C. Eom, J. S. Chang, C. Huh, G. Y. Sung, and J. H. Shin, Label-free optical biosensing using a horizontal air-slot SiNx microdisk resonator, Opt. Express **18**, 20638 (2010).
[21] M. Li, W. H. P. Pernice, and H. X. Tang, Ultrahigh-frequency nano-optomechanical resonators in slot waveguide ring cavities, Appl. Phys. Lett. **97**, 183110 (2010).
[22] M. Zhang, C. Wang, R. Cheng, A. Shams-Ansari, and M. Lončar, Monolithic ultra-high-Q lithium niobate microring resonator, Optica **4**, 1536 (2017).
[23] R. Wu, J. Zhang, N. Yao, W. Fang, L. Qiao, Z. Chai, J. Lin, and Y. Cheng, Lithium niobate micro-disk resonators of quality factors above 10^7, Opt. Lett. **43**, 4116 (2018).
[24] C. A. Barrios, Ultrasensitive nanomechanical photonic sensor based on horizontal slot-waveguide resonator, IEEE Photonics Technol. Lett. **18**, 2419 (2006).
[25] S. Lee, S. C. Eom, J. S. Chang, C. Huh, G. Y. Sung, and J. H. Shin, A silicon nitride microdisk resonator with a 40-nm-thin horizontal air slot, Opt. Express **18**, 11209 (2010).
[26] A. A. Savchenkov, A. B. Matsko, V. S. Ilchenko, and L. Maleki, Optical resonators with ten million finesse, Opt. Express **15**, 6768 (2007).
[27] X. Zhang, Q. Cao, Z. Wang, Y. Liu, C. Qiu, L. Yang, Q. Gong, and Y. Xiao, Symmetry-breaking-induced nonlinear optics at a microcavity surface, Nat. Photonics **13**, 21 (2019).
[28] W. C. Jiang and Q. Lin, Chip-scale cavity optomechanics in lithium niobate, Sci. Rep. **6**, 36920 (2016).
[29] Z. Fang, S. Haque, J. Lin, R. Wu, J. Zhang, M. Wang, J. Zhou, M. Rafa, T. Lu, and Y. Cheng, Real-time electrical tuning of an optical spring on a monolithically integrated ultrahigh q lithium niobate microresonator, Opt. Lett. **44**, 1214 (2019).